Hindawi
Advances in Civil Engineering
Volume 2018, Article ID 5791354, 11 pages
https://doi.org/10.1155/2018/5791354

Research Article

Parameter Sensitivity of Shallow-Bias Tunnel with a Clear Distance Located in Rock

Xueliang Jiang,[1,2] Feifei Wang,[1,2] Hui Yang,[1,2] and Jiayong Niu[1,2]

[1]*College of Civil Engineering, Central South University of Forestry and Technology, Changsha, Hunan 410004, China*
[2]*Rock and Soil Engineering Research Institute, Central South University of Forestry and Technology, Changsha, Hunan 410004, China*

Correspondence should be addressed to Feifei Wang; ffw1991@126.com

Received 25 October 2017; Revised 23 December 2017; Accepted 16 January 2018; Published 29 March 2018

Academic Editor: Dimitris Rizos

In order to obtain the seismic internal force response laws of a shallow-bias tunnel with a small clear distance, the reliability of the numerical simulation is verified by the shaking table model test. The parameter sensitivity of the tunnel is studied by using MIDAS-NX finite element software. The effects of seismic wave peak (0.1 g, 0.2 g, 0.3 g, 0.4 g, 0.5 g, and 0.6 g), existing slope angle (30°, 45°, 60°, and 90°), clear distance (1.0 D, 1.5 D, 2.0 D, and 3.0 D), and excitation mode (X direction, Z direction, XY direction, and XYZ direction) on the internal force response law of the tunnel are studied, respectively. The results show that (1) the shear force gradually increases with the increasing of seismic peak. The amplification is different with different measuring points. (2) Under different existing slope-angle conditions, the variation trend of shear force of the tunnel is similar, but the shear force is different. The existing slope has significant effect on the shear force response of the tunnel, and the degree is different with different slope angles. (3) Under the conditions of 1.5 D and 2.0 D, the shear force response of the tunnel is stronger, but the response of other conditions is relatively weak. The tunnel with 1.5 D to 2.0 D clear distance should be avoided. Different excitation modes have a significant effect on the shear force response of the tunnel. (4) Under the same excitation mode, the different excitation directions also have a significant effect on the shear force response. (5) The shear force response of the tunnel crosssection shows nonlinear variation trend. The shear force response is strongest at the arch shoulder and arch foot of the tunnel. The research results provide a useful reference for the design of antishock and vibration resistance of the tunnel.

1. Introduction

Tunnels have been important components of the transportation in mountain areas, which is beneficial to optimize the direction of the line and save construction cost. Previously, many scholars believed that the earthquake-resistant behavior of tunnels were stronger than that of aboveground buildings. After the earthquake observation, however, it is found that under the action of strong ground motion, tunnels may be subjected to extensive deformation or even collapse [1–4]. The surrounding rock has various pattern fractures, and a series of morphological changes occur in an earthquake [5–8]. Moreover, the dynamic response of tunnel structure is highly distinct from that of superstructure [9–11].

The dynamic response of underground structures (e.g., tunnels, culverts, underground stations, and underground reservoir structure) against earthquake has been a subject of intense study by the study methods of experiment [12–26] and numerical simulation [27–35] during recent years. From the above scholars' results, the study on seismic response of underground has achieved rich results. The research, however, mainly focuses on the dynamic response of the tunnel conventional type and underground structures.

The study, currently, on seismic force response of the new type tunnel (shallow-bias tunnel with a small distance) has a few been studied by scholars. The seismic force response of the new type tunnel is significantly different from that of the tunnel conventional type. The numerical methods (e.g., FEM, FDM, and BEM), as the most popular approaches, have been used to study the dynamic response of tunnels. A few experimental studies have been reported the acceleration response of the tunnel. Based on the comparison between the shaking table test and the numerical method, the results

obtained by the numerical method were credible and reasonable. This study aims to perform a systematic experimental work followed by means of an extended numerical parametric study to elaborate some dimensions of the problem. The effects of various parameters, including seismic wave peak (0.1 g, 0.2 g, 0.3 g, 0.4 g, 0.5 g, and 0.6 g), seismic wave excitation mode (X direction, Z direction, XZ direction, and XYZ direction), clear distance (1.0 D, 1.5 D, 2.0 D, and 3.0 D), and existing slope angle (30°, 45°, 60°, and 90°) on the seismic force response, were investigated in the present study.

2. Numerical Simulation

2.1. Eigenvalue Analysis. In order to calculate the mode shape and the natural period of undamped free vibration in MIDAS-NX, the characteristic equation is as follows:

$$K\Phi_n = \omega_n^2 M\Phi_n, \tag{1}$$

where K is the stiffness matrix of the structure, M is the mass matrix of the structure, ω_n^2 is the eigenvalue of the n mode, and Φ_n is the mode vector of the n mode.

Eigenvalue analysis, also known as free vibration analysis, is used to analyze the inherent dynamic characteristics of structures. By eigenvalue analysis, the main dynamic characteristics, such as mode shape, natural vibration period, and vibration mode participation coefficient, are determined by the structure quality and stiffness.

In the calculation, the load and damping in the equation of motion of the SDOF system are assumed to be 0. Then the equation degenerates into free vibration equation, which is as follows:

$$\begin{aligned} m\ddot{u} + c\dot{u} + ku &= p(t), \\ m\ddot{u} + ku &= 0, \end{aligned} \tag{2}$$

where u is the displacement induced by vibration. If $u = A\cos\omega t$ (A is related to the initial displacement constant), (2) can be changed into the following formula:

$$\left(-m\omega^2 + k\right)A\cos\omega t. \tag{3}$$

The conditions of (2) are that the item in parentheses is 0. So the eigenvalues are as follows:

$$\begin{aligned} \omega^2 &= \frac{k}{m}, \\ \omega &= \sqrt{\frac{k}{m}}, \\ f &= \frac{\omega}{2\pi}, \\ T &= \frac{1}{f}, \end{aligned} \tag{4}$$

where ω^2 is the eigenvalue, ω is the proper circular frequencies, T is the natural period, and f is the natural frequency.

The vibration mode participation coefficient is calculated by the ratio of response between the mode shape and all involved vibration modes. The calculation formula is as follows:

$$\tau_m = \frac{\sum M_i\varphi_{im}}{\sum M_i\varphi_{im}^2}, \tag{5}$$

where M is the order of the mode shapes, τ_m is the mode participation coefficient, M_i is the quality of i nodes, and φ_{im} is the m order vibration vector of i node position.

In order to ensure that the earthquake mainly contains enough vibration, modal effective mass M is greater than the sum of all the effective mass of 90% general provisions in the seismic design code.

$$M_m = \frac{\left[\sum\varphi_{im}M_i\right]}{\sum\varphi_{im}^2 M_i}, \tag{6}$$

where M_m is the effective mass of various modes.

2.2. Computation Damping. The Rayleigh damping type is used in the numerical simulation. In order to reduce the uncertainty of stiffness damping in the high modes, the sum of both mass proportional damping and stiffness damping is used as the damping matrix.

The proportional damping matrix C adopts the formula proposed by Caughey:

$$C = M\left\{\sum_{j=0}^{N-1} a_j\left(M^{-1}K\right)^j\right\}, \tag{7}$$

where j and N are the nodal degrees of freedom. $M^{-1}K$ can be calculated by the free vibration formula of the undamped system:

$$M\{y\} + K\{y\} = 0, \tag{8}$$

$$\{y\} = \{u\}e^{iax}. \tag{9}$$

Substituting formula (9) in (8), the following formula can be obtained:

$$\left(-\omega^2 M + K\right)\{u\} = \{0\}. \tag{10}$$

In $M^{-1}K = \omega^2$, ω^2 is equivalent to the number of modes, and it is expressed by ω_s^2.

Substituting $M^{-1}K$ in formula (7) and multiplying (7) by $\{u_s\}^T$ and u_s on both sides, the following formula can be obtained:

$$\{u_s\}^T C\{u_s\} = C_s = \sum_{j=0}^{N-1} a_j\omega_s^{2j}\{u_s\}^T M\{u_s\} = \sum_{j=0}^{N-1} a_j\omega_s^{2j}M_s. \tag{11}$$

The damping constant h_s of the s order vibration mode is expressed by the following formulas (12) and (13):

$$C_s = 2h_s\omega_s M_s, \tag{12}$$

$$\begin{aligned} h_s &= \frac{C_s}{2\omega_s M_s} = \frac{1}{2\omega_s}\sum a_j\omega_s^{2j} \\ &= \frac{1}{2}\left(\frac{a_0}{\omega_s} + a_1\omega_s + a_2\omega_s^3 + \cdots + a_{N-1}\omega^{2N-3}\right), \\ s &= 1 - N. \end{aligned} \tag{13}$$

The damping constant of the mass ratio and stiffness type is shown in the following formulas (14) and (15), respectively.

The Rayleigh damping matrix is shown in the following formula (16).

Mass proportion type:

$$h_s = \frac{a_0}{2\omega_s}, \quad C = a_0 M. \tag{14}$$

Stiffness proportional type:

$$h_s = \frac{a_1 \omega_s}{2}, \quad C = a_0 M. \tag{15}$$

Rayleigh type:

$$h_s = \frac{a_1 \omega_s}{2}, \quad C = a_0 M. \tag{16}$$

2.3. Time History Analysis. The structural dynamic time history analysis refers to the process of calculating the structural response (displacement, velocity, internal force, etc.) at any moment, when the structure is subjected to dynamic loads. The dynamic equilibrium equation is used in the dynamic time history analysis of MIDAS-NX, which is as follows:

$$[M]\ddot{u}(t) + [C]\dot{u}(t) + [K]u(t) = p(t), \tag{17}$$

where $[M]$ is the mass matrix, $[C]$ is the damping matrix, $[K]$ is the stiffness matrix, $p(t)$ is the dynamic loading, $\ddot{u}(t)$ is the relative acceleration, $\dot{u}(t)$ is the relative velocity, and $u(t)$ is the relative displacement.

The modal superposition method for structural dynamic analysis is used to carry out dynamic time history analysis in MIDAS-NX. The mode superposition method means that the displacement of the structure is solved by a linear combination of orthogonal displacement vectors. This method is better for linear dynamic analysis of large structures. The premise of using this method is that the damping matrix can be represented by a linear combination of the mass matrix and the stiffness matrix.

The mode superposition method is one of the most widely used methods of structural analysis program. But in nonlinear dynamic analysis, this method has some limitations. In order to make up for this shortcoming, the nonlinear characteristics of stiffness and damping can be taken into account in MIDAS-NX. In nonlinear dynamic time history analysis, the direct integration method is adopted. The direct integral method is a method of time as the integral parameter solution of the dynamic equilibrium equation. Analysis of dynamic time history using the Newmark method with better convergence in MIDAS-NX is performed. The basic integral method is as follows:

$$\dot{u}_{t+\Delta t} = \dot{u}_t + \left[(1-\delta)\ddot{u}_t + \delta^{t+\Delta t}\ddot{u}\right]\Delta t, \tag{18}$$

$$u_{t+\Delta t} = u_t + \dot{u}_t \Delta t + \left[\left(\frac{1}{2} - \alpha\right)\ddot{u}_t + \alpha\ddot{u}_{t+\Delta t}\right]\Delta t^2, \tag{19}$$

$\ddot{u}_{t+\Delta t}$ can be obtained from (19). It is substituted in formula (18), and $\dot{u}_{t+\Delta t}$ is calculated to obtain the relationship between displacement, velocity, and acceleration of the current stage and that of the last stage as follows:

$$\begin{aligned} \ddot{u}_{t+\Delta t} &= f\left(u_{t+\Delta t},\ u_t, \dot{u}_t, \ddot{u}_t\right), \\ \dot{u}_{t+\Delta t} &= f\left(u_{t+\Delta t},\ u_t, \dot{u}_t, \ddot{u}_t\right), \end{aligned} \tag{20}$$

$$[M]\ddot{u}_{t+\Delta t}[C]\dot{u}_{t+\Delta t} + [K]u_{t+\Delta t} = p^{t+\Delta t}. \tag{21}$$

Substituting formula (20) in formula (21), the present displacement can be obtained. The present velocity and acceleration can be obtained by present and last displacements:

$$\begin{aligned} &\left[[K] + a_0[M] + a_1[C]\right]u_{t+\Delta t} \\ &\quad = p_{t+\Delta t} + [M]\left(a_0 u_t + a_2\dot{u}_t + a_3\ddot{u}_t\right) \\ &\qquad + [C]\left(a_1 u_t + a_4\dot{u}_t + a_5\ddot{u}_t\right), \end{aligned} \tag{22}$$

$$[\widehat{K}]u_{t+\Delta t} = \widehat{p}_{t+\Delta t}, \tag{23}$$

$$\begin{aligned} [\widehat{K}] &= [K] + a_0[M] + a_1[C], \\ \widehat{p}_{t+\Delta t} &= p_{t+\Delta t} + [M]\left(a_0 u_t + a_2\dot{u}_t + a_3\ddot{u}_t\right) \\ &\quad + [C]\left(a_1 u_t + a_4\dot{u}_t + a_5\ddot{u}_t\right) \\ \ddot{u}_{t+\Delta t} &= a_0\left(u_{t+\Delta t} - u_t\right) - a_2\dot{u}_t - a_3\ddot{u}_t, \\ \ddot{u}_{t+\Delta t} &= \dot{u}_t + a_6\ddot{u}_t + a_7\ddot{u}_{t+\Delta t}, \end{aligned} \tag{24}$$

where $a_0 = 1/\alpha\Delta t^2, a_1 = \delta/\alpha\Delta t, a_2 = 1/\alpha\Delta t, a_3 = 1/2\alpha - 1, a_4 = \delta/\alpha - 1, a_5 = \Delta t/2\,(\delta/\alpha - 2), a_6 = \Delta t\,(1-\delta), a_7 = \delta\Delta t$, and α and β are the integral parameters of Newmark ($\alpha = 0.5$, $\beta = 0.25$). Δt is the integral time interval.

Midas-NX analysis software based on finite element theory can transform differential equations into linear algebraic equations to solve problems. It is applicable to anisotropic, nonlinear, and heterogeneous materials and has an effective applicability for complex boundary conditions. It can better reveal the dynamic response law of tunnel under earthquake loading. In this paper, Midas-NX finite element software is used to analyze the nonlinear dynamic response of the tunnel. In order to reduce the boundary effect in numerical simulation, the model size is more than 5 times the diameter of the tunnel. Therefore, the length, width, and height of the numerical model are 60 m, 40 m, and 55 m, respectively.

Lysmer and Kuhlemeyer [36] showed that for accurate representation of wave transmission through a model, the element size Δ_l must be smaller than approximately 1/10 to 1/8 of the wavelength associated with the highest frequency component of the input wave:

$$\Delta_l \leq \frac{\lambda}{10} \text{ to } \frac{\lambda}{8}, \tag{25}$$

where λ is the wavelength of the propagated wave in the model.

According to the calculation results, the total number of nodes and units in the numerical calculation model are 9,548

and 42,539, respectively. In the numerical simulation, the surrounding rock and the lining are simulated by a solid element, and the elastic-plastic constitutive model and Mohr-Coulomb yield criterion are used. In the computational model, the free field boundary and Rayleigh damping are used, and the critical damping ratio of 5% is considered. The specific calculation model is shown in Figure 1.

The Darui artificial wave is used as the loading wave. The time history curve of acceleration of the Darui artificial wave and its Fourier spectrum are shown in Figure 2. Five measuring points are respectively located at the arch foot, arch shoulder, and vault of each lining inside the double hole. LF and RF refer to the left arch foot and right arch foot, respectively. LS and RS refer to the left arch shoulder and right arch shoulder, respectively. VA refers to vault. The number of measuring points is 1~5 and 6~10 in the left hole and right hole, respectively. The detailed measuring points are shown in Figure 3. The physical and mechanical parameters of the surrounding rock and lining model are given in Table 1.

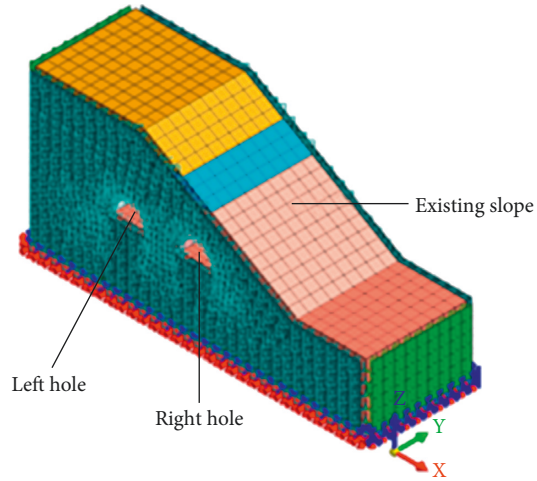

Figure 1: Numerical calculation model.

3. Analysis of Calculation Results

3.1. Verification of Shaking Table Test. In order to verify the reliability of numerical simulation, a series of large-scale shaking table physical model tests have been carried out at the National Engineering Laboratory of the high-speed railway construction technology in Central South University (Figure 4). In the model test, the static and dynamic parameters of the model and prototype must satisfy the similarity relation. The factors such as the size of the shaking table, the relevant parameters of the test instrument, the carrying capacity, and the model boundary effect are comprehensively considered. Finally, the geometric similarity ratio of the model is 1 : 10; the acceleration similarity ratio is 1 : 1; and the density similarity ratio is 1 : 1. Other main similarity constants can be deduced from similarity theory and dimensional analysis.

The rigid model box was used in the shaking table test, which was made of a steel plate, section steel, and plexiglass material (Figure 4). In order to eliminate the boundary effect of the model box, the middle sand and crushed stone were used as the friction boundary at the bottom of the model box. The polystyrene foam was pasted on the inner wall of the model box. A layer of PVC film was pasted on the polystyrene foam board at the left and right sides of the model box. The boundary of the model was dealt within literature [37, 38].

The lining model was made of microconcrete which was similar to the physical properties of concrete. Steel bar is simulated with a galvanized iron wire. According to the similarity constant, the lining thickness is determined to be 4 cm. After several times of proportioning test, the optimum lining model material ratio is 1 : 6.9 : 1.3 (cement : sand : water). The compressive strength of lining is converted to 5 MPa in accordance with the stress similitude ratio. The surrounding rock of the tunnel is divided into three layers. The first layer is weakly weathered rock; second layer is weak rock; and third layer is hard rock. The mixed proportion of similar materials from top to bottom is 1 : 6.30 : 1.17 (cement : sand : water) of M7.5 mortar, 1 : 7.25 : 1.35 (cement : sand : water) of M5 mortar, and 1 : 5.58 : 1.04 (cement : sand : water) of M10 mortar, respectively. The buried depth of the tunnel is 0.9 m; the clear width of the tunnel is 0.7 m; and thickness of the middle partition wall is 0.4 m.

The acceleration sensor was used to record the response of the measuring point in the shaking table test. The type, range, and sensitivity were 1221L-002, 1221L-002, ±20 m·s^{-2}, and 2000 mv/g, respectively. The location and number of measuring points in shaking table test is the same as that in numerical simulation. One measuring point was used as the reference point, which was located at the shaking table, and the number is 11.

The reliability of numerical simulation is verified by the acceleration response of the tunnel. The 0.4 g Darui artificial wave (DR-XZ) curves of the shaking table test and numerical simulation are shown in Figure 5. In the 0.4 g condition, the acceleration response peak of each measuring point in horizontal and vertical directions is shown in Table 2.

As shown in Figure 4, the time history curves of the shaking table test and numerical simulation are similar, indicating that the numerical simulation is in good agreement with the shaking table test. As shown in Table 2, the acceleration response peak value obtained by vertical simulation calculation is basically consistent with the peak value obtained by the shaking table test. The error is within the reasonable range. The results show that the shaking table test results are reasonable and the numerical simulation results are reliable.

3.2. Analysis of Tunnel Shear Force with Different Slope Angles. In this paper, shear force is taken as an index to investigate the difference of dynamic response of the tunnel under different existing slope-angle conditions (30°, 45°, 60°, and 90°). Numerical calculation results show the variation trends of shear force, which are shown in Figure 6.

As shown in Figure 6(a), the shear force at the arch foot and vault of the tunnel is smaller, while the shear force at the arch shoulder is larger. The overall variation trend of each hole presents an "M" shape. At the same measuring point,

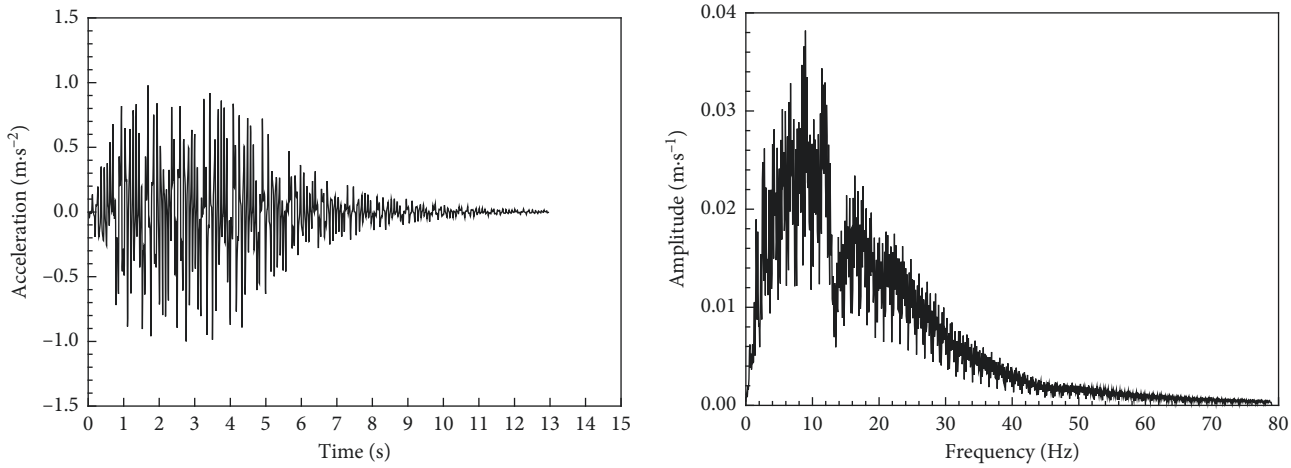

Figure 2: (a) The time history curve of acceleration of the Darui artificial wave and (b) its Fourier spectrum.

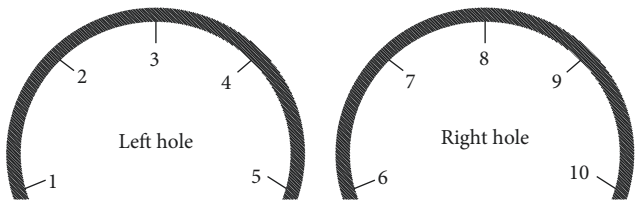

Figure 3: Measuring points.

Figure 4: Shaking table test.

Table 1: Physical and mechanical parameters of the surrounding rock and lining model.

Materials	E (MPa)	μ	Φ (°)	C (kPa)	γ (kN·m^{-3})
Weakly weathered rock	600	0.25	39	70	23
Weak rock	130	0.3	27	20	20
Hard rock	1890	0.3	50	150	25
Lining	3450	0.167	—	—	24

E, elastic modulus; μ, Poisson ratio; Φ, internal friction angle; C, cohesion; γ, bulk density.

the shear force varies greatly with different loading peaks. The shear force increases with the increase of the seismic wave peak. Under the seismic wave peak of 0.1 g, the maximum of shear force at arch shoulder is 30 kN. Under the seismic wave peak of 0.6 g, the maximum of shear force at spandrel is 210 kN, which increases by 6 times. Therefore seismic wave peak has a significant influence on the shear force of the tunnel crosssection. The shear forces at both left arch shoulder and right arch shoulder are the same in the left hole, and the result is 180 kN. The arch shoulders of the right hole have different shear force. The result of the left arch shoulder is 140 kN, but the result of the right arch shoulder is 210 kN. And the difference is 70 kN. The reason is that the upper rock layer of the left hole is thick and has good stability, and it is far away from the existing slope and is less affected by the existing slope. The right hole is close to the existing slope, and the slope has a great influence on the seismic force response of the right tunnel under the earthquake dynamic action. The right arch shoulder of the right hole is close to the existing slope, and the upper rock layer has poor stability.

By comparing Figures 6(a)–6(d), it can be seen that the variation trend of shear force of the tunnel crosssection is similar under different existing slope-angle conditions, but the shear strength is different. It can be seen that the existing slope angle never changes the seismic force response characteristics of the tunnel but only affects the response intensity of the seismic force. With the increase of the existing slope angle, the difference of shear force between the two arches gradually increases in the left hole. The difference of shear force between the two arches gradually decreases in the right hole. When the existing slope angle is 90°, the shear strength of the left hole is the same as that of the right hole. The variation trend presents symmetrical distribution. It can be seen that the existing slope has significant influence on the seismic force response of the tunnel. The degree of influence is different under different existing slope angles. In actual engineering practice, the influence of the existing slope angle on the dynamic stability of the tunnel should be fully considered.

3.3. Analysis of Tunnel Shear Force with Different Clear Distances. In this paper, shear force is taken as an index to

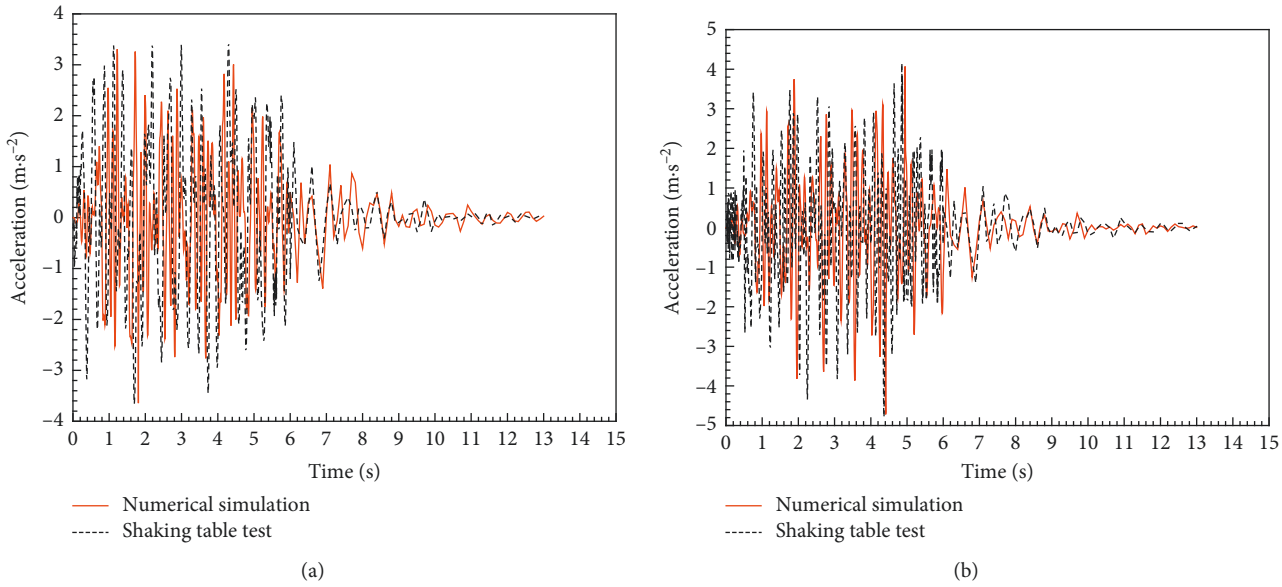

Figure 5: Time history curves of numerical simulation and shaking table test. (a) Horizontal direction. (b) Vertical direction.

Table 2: Comparison of acceleration response peak value (unit: m·s^{-2}).

Measuring points	X		Z	
	Shaking table test	Numerical simulation	Shaking table test	Numerical simulation
1	3.12	3.21	5.05	5.03
2	1.56	1.62	2.49	2.32
3	3.66	3.60	4.68	4.60
4	4.19	4.17	1.83	1.93
5	4.06	4.19	4.17	4.18
6	1.79	1.90	5.08	5.07
7	3.84	3.89	4.71	4.81.
8	1.56	1.72	5.22	5.13
9	4.16	4.01	4.88	4.81
10	6.75	6.60	4.99	4.98

investigate the difference of seismic force response of the tunnel under different clear distance conditions (1.0 D, 1.5 D, 2.0 D, and 2.5 D, where D is the tunnel diameter). The shear force is calculated, and variation trends of shear force are shown in Figure 7.

By Figure 7(a), it can be seen that the shear force of the left hole firstly increases, then decreases, and finally increases. The variation trend of shear force of the right hole is complex. There are differences in the variation trend between left and right holes. The main reason is the influence of the existing slope on the right tunnel. The shear force at the arch shoulder and arch foot is larger. The maximum is 330 kN in 0.6 g condition. At the vault, the shear force is small. The seismic force response of the left hole is larger than that of the right hole. The reason is that the overburden thickness of the left hole is larger than that of the right hole. The inertia force of the left hole is larger under the action of seismic wave. Under the condition of 1.5 D and 2.0 D, the maximum at the right arch foot of the left hole is 920 kN. Under the 3.0 D condition, the maximum at the right arch foot of the left hole is 750 kN.

By comparing the four conditions' (1.0 D, 1.5 D, 2.0 D and 3.0 D, where D is the tunnel diameter) variation trend of shear force response and response values, it is found that under 1.5 D and 2.0 D conditions the seismic force response of the tunnel crosssection is strong, while the 1.0 D and 3.0 D response is relatively weak. This conclusion can provide reference for practical engineering examples of small clear distance tunnels and avoid constructing tunnels with 1.5 D to 2.0 D spacing as far as possible. The magnitude of the shear force response of the tunnel crosssection is affected by the seismic wave peak. The seismic force response increases with the increase of the seismic wave peak. A linear variation is presented.

3.4. Analysis of Tunnel Shear Force with Different Loading Modes. Under different loading modes, the shear force is taken as an index to investigate the difference of seismic force response of the tunnel (X direction, Z direction, XZ direction, and XYZ direction). X is the horizontal direction, Y is the tunnel axis direction, and Z is the vertical direction. The shear force is calculated, and variation trends of shear force are shown in Figure 8.

As shown in Figure 8(a), the shear force of the tunnel crosssection shows an "M" shape trend under the action of one-way loading wave (X direction). Under the same loading peak, the shear force reaches the maximum at the arch shoulder, and the maximum is 218 kN. The minimum is in the arch foot and vault. Because of the influence of the existing slope on the shear force response of the tunnel, the variation trends of the shear force in the left and right tunnels never show a symmetrical trend.

As shown in Figure 8(b), the shear force of the tunnel crosssection shows a "V" shape trend under the action of one-way loading wave (Z direction). Under the same loading

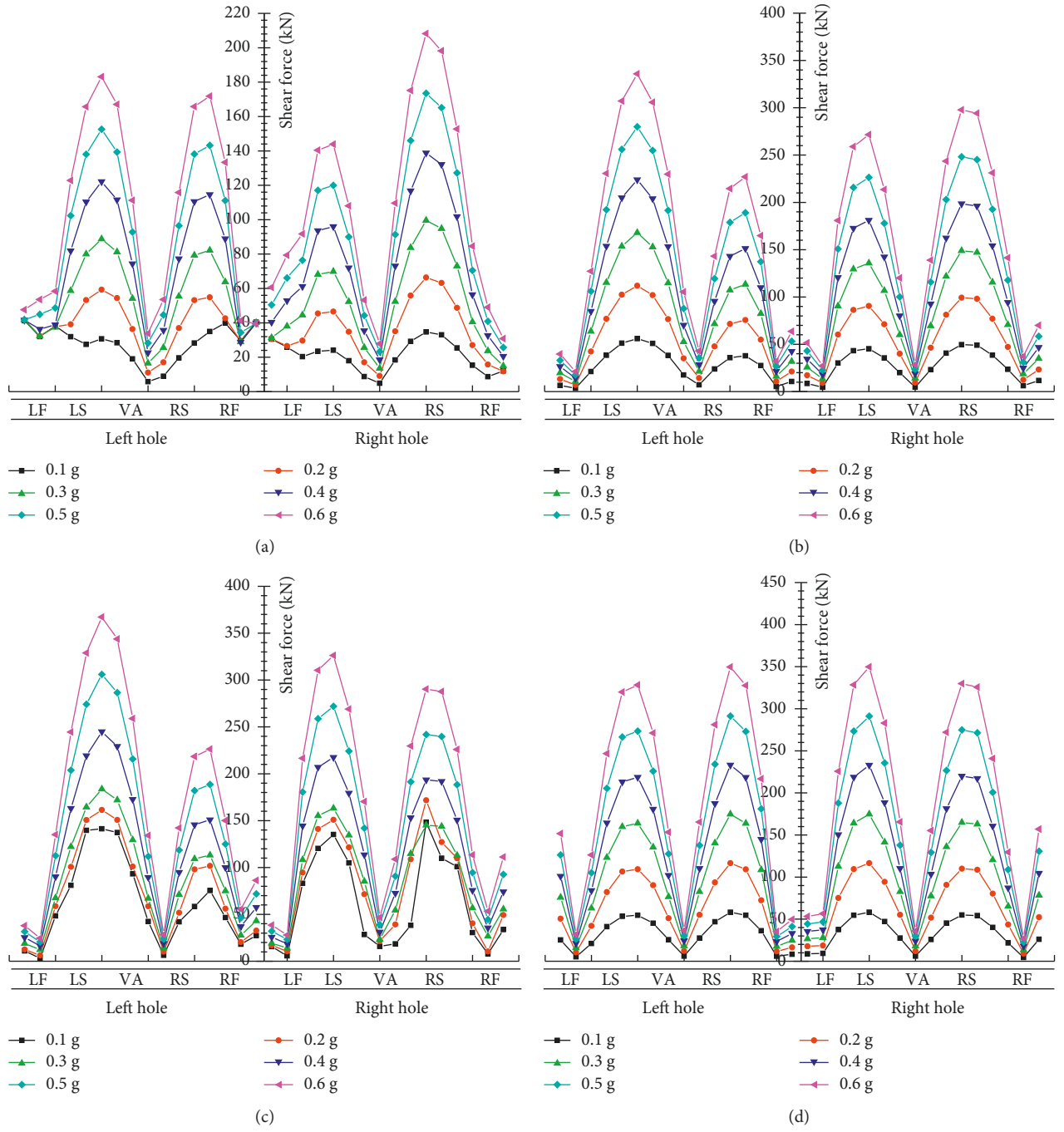

Figure 6: Shear force of tunnel crosssection of different existing slope angles. (a) 30°, (b) 45°, (c) 60°, and (d) 90°d.

peak, the shear force reaches the maximum at the arch foot, and the maximum is 280 kN. The minimum is in the vault. Because of the influence of the existing slope on the shear force response of the tunnel, the variation trends of the shear force of the left and the right holes never show a symmetrical trend, and the response of the left hole is more intense. The main reason is that in the vertical direction of loading wave (Z direction), the overlying strata of the left hole are thicker; the action force of the left hole is greater; and the "rise effect" has a significant impact on the shear force response of the left hole. By comparing Figures 6(a) and 6(b), it can be seen that the loading direction of the single direction loading method is different, and the magnitude and variation trend of tunnel shear force are different. It shows that the loading direction of seismic wave has a significant influence on the seismic force response of the tunnel.

From Figure 8(c), it can be seen that under the action of bidirectional wave loading (XZ), the variation trend of shear force is more complex. The left hole shows the trend of first increasing, then decreasing, and final increasing, and the maximum is located at the arch shoulder and arch foot. The shear force of the right tunnel is larger at the arch shoulder

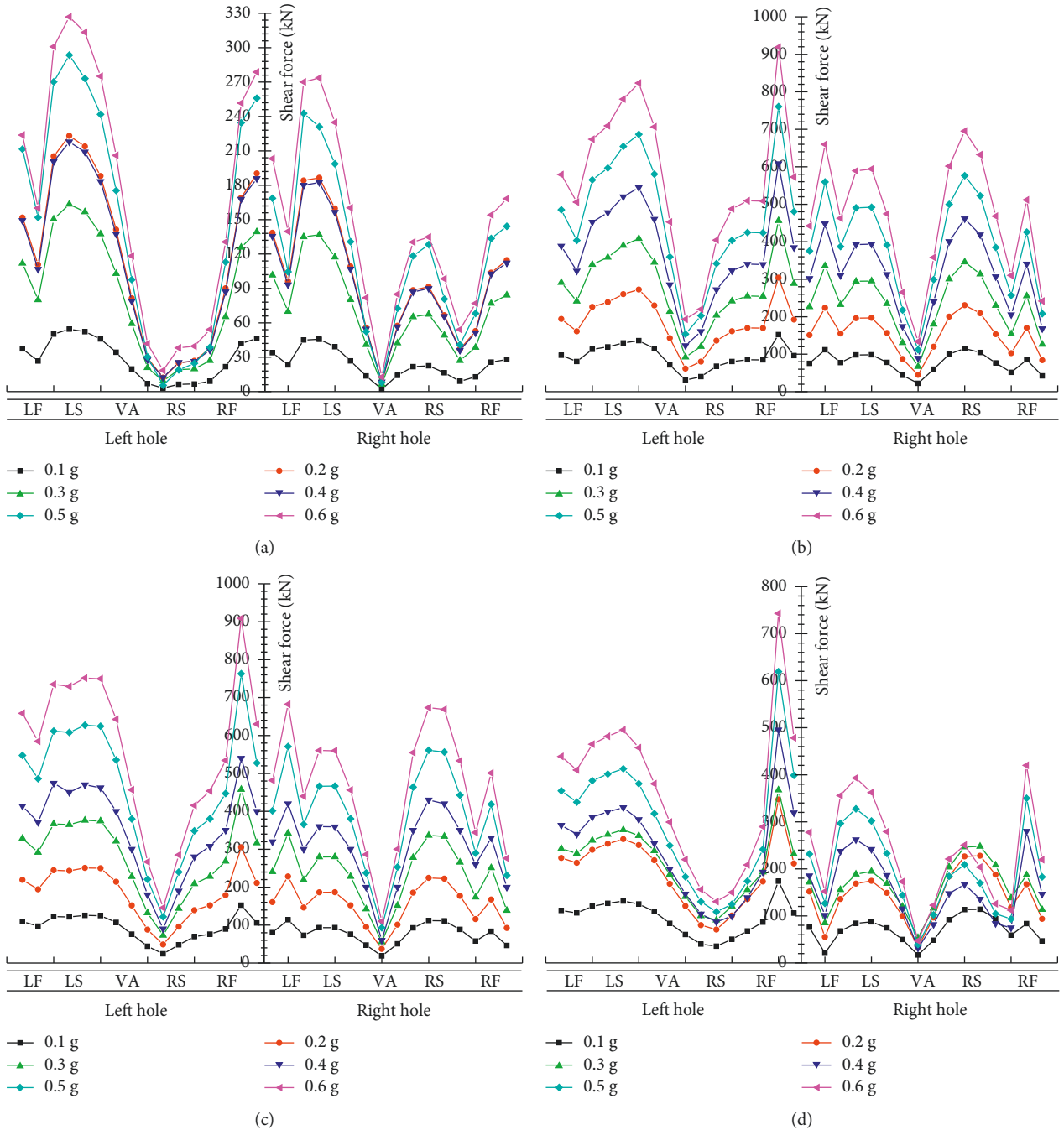

Figure 7: Shear force of the tunnel crosssection of different clear distances. (a) 1.0 D, (b) 1.5 D, (c) 2.0 D, and (d) 3.0 D.

and arch foot. The left half arch shear force is larger than the right half arch in the right hole. The reason may be that the response of the vertical direction is stronger than that of the horizontal direction under the action of the bidirectional wave. In the vertical direction, the response of the right arch is weaker than that of the left half arch, and it is affected by the dynamic response of the middle rock column due to the close distance between the left arch and the middle rock column.

As shown in Figure 8(d), the variation trend of shear force is complex under the action of bidirectional wave loading (XYZ). The shear force at the arch foot and the arch shoulder is larger, and the vault is smaller. The maximum is located at the right arch foot of the left hole. Under 0.6 g loading peak, the maximum is 700 kN. The variation tends at both the left hole and the right hole are similar, but the numerical value of shear force is different. The reason may be that the seismic wave acts as the main factor under the action of the three directions of seismic waves, while the influence of the existing slope weakens.

By comparing Figures 7(a)–7(d), it can be seen that the seismic wave peak has an effect on the shear force of the

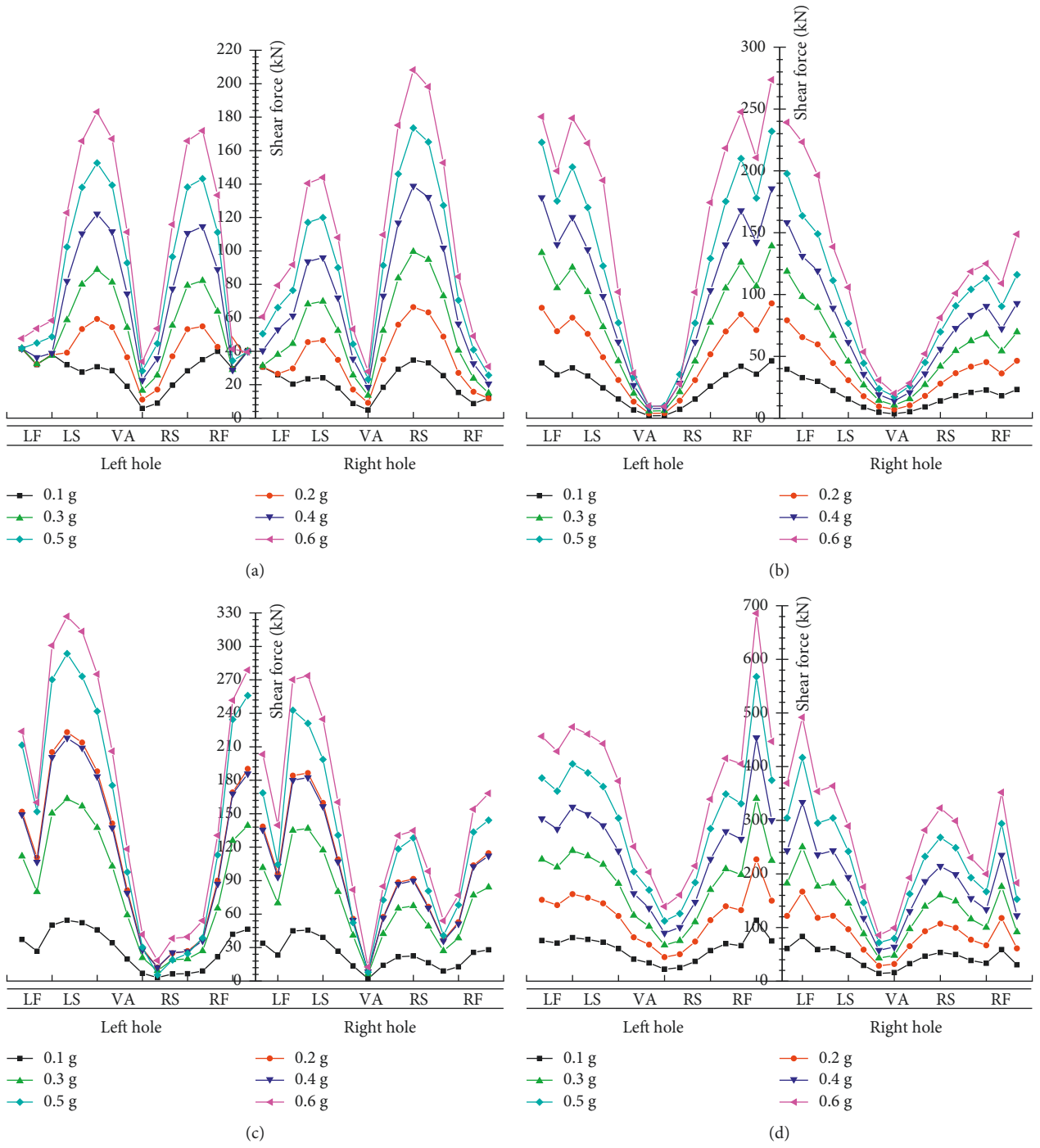

Figure 8: Shear force of the tunnel crosssection with different loading modes. (a) X direction; (b) Z direction; (c) XZ direction; (d) XYZ direction.

tunnel crosssection. With the increase of the excitation peak value, the shear force increases gradually. The transverse shear force of the small clear distance tunnel shows nonlinear variation trend. Different loading modes have a significant influence on the shear force response. Under the same loading mode, the different loading directions also have a significant influence on the shear force response. The maximum shear force occurs at the arch shoulder and arch foot of the tunnel. Therefore, the seismic fortification measures should be strengthened at the arch shoulder and arch foot of the tunnel.

4. Conclusions

The reliability of the numerical simulation is verified by the shaking table model test. The parametric study of a shallow-bias tunnel with a clear distance is carried out by using

MIDAS-NX finite element software. The tunnel shear responses under different seismic wave peaks (0.1 g, 0.2 g, 0.3 g, 0.4 g, 0.5 g, and 0.6 g), different loading modes (X direction, Z direction, XZ direction and XYZ direction), different existing slope angles (30, 45, 60 and 90°), and different clear distances (1.0 D, 1.5 D, 2.0 D and 2.5 D) are studied. The following conclusions are obtained:

(1) The shear force gradually increases with the increasing of seismic peak. The amplification is different with different measuring points. Moreover, the variation trend is invariable, although the conditions (such as different loading modes, different existing slope angles, and different clear distances) are different.

(2) Under different existing slope-angle conditions, the variation trend of shear force of tunnel crosssection is similar, but the shear strength is different. The existing slope angle never changes the seismic force response characteristics of the tunnel, but only affects the seismic force response. With the increase of the existing slope angle, the difference of shear strength of the arch is becoming larger in the left hole. However, the difference in the right hole decreases gradually. The existing slope has a significant influence on the seismic force response of the tunnel, and the influence degree is different under different existing slope angles. In actual engineering practice, the influence of the existing slope angle on the dynamic stability of the tunnel should be fully considered.

(3) Under different clear distance conditions, the shear force at the arch shoulder and arch foot are larger, while the shear force at the vault is smaller. Under 1.5 D and 2.0 D conditions, the shear force response of the tunnel crosssection is stronger. The shear force response of 1.0 D and 3.0 D is relatively weak. In practical engineering examples, the tunnels with 1.5 D to 2.0 D clear distance should be avoided as far as possible.

(4) Under different loading modes, the shear force response of tunnel is different. Under the same loading mode, the shear force response in different loading directions is different. The loading mode of the seismic wave has a significant influence on the shear force of the tunnel crosssection.

(5) The shear force response of the tunnel crosssection shows nonlinear variation trend. The shear force response is strongest at the arch shoulder and arch foot of the tunnel. Therefore, it is necessary to strengthen the seismic fortification measures at the key point.

Conflicts of Interest

The authors declare that they have no conflicts of interest.

Acknowledgments

The authors are grateful for financial support from the National Natural Science Foundation (NNSF) of China through Grant nos. 51204215 and 51404309.

References

[1] W. L. Wang, T. T. Wang, J. J. Su, C. H. Lin, C. R. Seng, and T. H. Huang, "Assessment of damage in mountain tunnels due to the Taiwan Chi-Chi earthquake," *Tunnelling and Underground Space Technology*, vol. 16, no. 3, pp. 133–150, 2001.

[2] Y. M. A. Hashash, J. J. Hook, B. Schmidt, and J. I. C. Yao, "Seismic design and analysis of underground structures," *Tunnelling and Underground Space Technology*, vol. 16, no. 4, pp. 247–293, 2001.

[3] Y. J. Jiang, C. X. Wang, and X. D. Zhao, "Damage assessment of tunnels caused by the 2004 Mid Niigata prefecture earthquake using Hayashi's quantification theory type II," *Natural Hazards*, vol. 53, no. 3, pp. 425–441, 2010.

[4] Z. Z. Wang and Z. Zhang, "Seismic damage classification and risk assessment of mountain tunnels with a validation for the 2008 Wenchuan earthquake," *Soil Dynamics and Earthquake Engineering*, vol. 45, no. 2, pp. 45–55, 2013.

[5] Y. L. Zhao, L. Y. Zhang, W. J. Wang, J. Tang, H. Lin, and W. Wan, "Transient pulse test and morphological analysis of single rock fractures," *International Journal of Rock Mechanics and Mining Sciences*, vol. 91, pp. 139–154, 2017.

[6] Y. Zhao, Y. Wang, W. Wang, W. Wan, and J. Tang, "Modeling of non-linear rheological behavior of hard rock using triaxial rheological experiment," *International Journal of Rock Mechanics and Mining Sciences*, vol. 93, pp. 66–75, 2017.

[7] Y. Zhao, L. Zhang, W. Wang et al., "Creep behavior of intact and cracked limestone under multi-level loading and unloading cycles," *Rock Mechanics and Rock Engineering*, vol. 50, no. 6, pp. 1–16, 2017.

[8] Y. Zhao, J. Tang, Y. Chen et al., "Hydromechanical coupling tests for mechanical and permeability characteristics of fractured limestone in complete stress–strain process," *Environmental Earth Sciences*, vol. 76, pp. 1–18, 2016.

[9] Q. Q. Gao, *The Memoir on Tunnel & Underground Structure of Gao Quqing*, China Railway Publishing House, Beijing, China, 1996.

[10] G. Lin, "Summarization on anti-seismatic analysis of underground structure (A)," *World Earthquake Engineering*, vol. 6, no. 2, pp. 1–9, 1990.

[11] G. Lin, "Summarization on anti-seismatic analysis of underground structure (B)," *World Earthquake Engineering*, vol. 6, no. 3, pp. 1–10, 1990.

[12] J. C. Chou, B. L. Kutter, T. Travasarou, and J. M. Chacko, "Centrifuge modeling of seismically induced uplift for the BART Transbay tube," *Journal of Geotechnical and Geoenvironmental Engineering*, vol. 137, no. 8, pp. 754–765, 2010.

[13] S. Shibayama, J. Izawa, A. Takahashi, J. Takemura, and O. Kusakabe, "Observed behavior of a tunnel in sand subjected to shear deformation in a centrifuge," *Soils and Foundations*, vol. 50, no. 2, pp. 281–294, 2010.

[14] S. C. Chian and S. P. G. Madabhushi, "Effect of buried depth and diameter on uplift of underground structures in liquefied soils," *Soil Dynamics and Earthquake Engineering*, vol. 41, pp. 181–190, 2012.

[15] U. Cilingir and S. P. G. Madabhushi, "A model study on the effects of input motion on the seismic behavior of tunnels," *Soil Dynamics and Earthquake Engineering*, vol. 31, no. 3, pp. 452–462, 2011a.

[16] U. Cilingir and S. P. G. Madabhushi, "Effect of depth on the seismic response of square tunnels," *Soils and Foundations*, vol. 51, no. 3, pp. 449–457, 2011b.

[17] U. Cilingir and S. P. G. Madabhushi, "Effect of depth on the seismic response of circular tunnels," *Canadian Geotechnical Journal*, vol. 48, no. 1, pp. 117–127, 2011c.
[18] G. Lanzano, E. Bilotta, G. Russo, F. Silvestri, and S. P. G. Madabhushi, "Centrifuge modeling of seismic loading on tunnels in sand," *Geotechnical Testing Journal*, vol. 35, no. 6, pp. 854–869, 2012.
[19] G. Chen, Z. Wang, X. Zuo, X. Du, and H. Gao, "Shaking table test on seismic failure characteristics of a subway station structure in liquefiable ground," *Earthquake Engineering & Structural Dynamics*, vol. 42, pp. 1489–1507, 2013.
[20] G. Tsinidis, K. Pitilakis, G. Madabhushi, and C. Heron, "Dynamic response of flexible square tunnels: centrifuge testing and validation of existing design methodologies," *Geotechnique*, vol. 65, no. 5, pp. 401–417, 2015.
[21] O. Abuhajar, H. El Naggar, and T. Newson, "Seismic soil-culvert interaction," *Canadian Geotechnical Journal*, vol. 52, pp. 1649–1667, 2015a.
[22] O. Abuhajar, H. El Naggar, and T. Newson, "Experimental and numerical investigations of the effect of buried box culverts on earthquake excitation," *Soil Dynamics and Earthquake Engineering*, vol. 79, pp. 130–148, 2015b.
[23] D. Ulgen, S. Saglam, and M. Y. Ozkan, "Dynamic response of a flexible rectangular underground structure in sand: centrifuge modeling," *Bulletin of Earthquake Engineering*, vol. 13, pp. 2547–2566, 2015.
[24] A. Hushmand, S. Dashti, C. Davis, J. S. McCartney, and B. Hushmand, "A centrifuge study of the influence of site response, relative stiffness, and kinematic constraints on the seismic performance of buried reservoir structures," *Soil Dynamics and Earthquake Engineering*, vol. 88, pp. 427–438, 2016.
[25] G. Tsinidis, K. Pitilakis, and G. Madabhushi, "On the dynamic response of square tunnels in sand," *Engineering Structures*, vol. 125, pp. 419–437, 2016.
[26] G. Tsinidis, E. Rovithis, K. Pitilakis, and J. L. Chazelas, "Seismic response of box-type tunnels in soft soil: experimental and numerical investigation," *Tunnelling and Underground Space Technology*, vol. 59, pp. 199–214, 2016.
[27] Y. M. A. Hashash, D. Park, and J. I. C. Yao, "Ovaling deformations of circular tunnels under seismic loading, an update on seismic design and analysis of underground structures," *Tunnelling and Underground Space Technology*, vol. 20, no. 5, pp. 435–441, 2005.
[28] H. Huo, A. Bobet, G. Fernández, and J. Ramírez, "Load transfer mechanisms between underground structure and surrounding ground: evaluation of the failure of the Daikai station," *Journal of Geotechnical and Geoenvironmental Engineering*, vol. 131, no. 12, pp. 1522–1533, 2005.
[29] I. Anastasopoulos, N. Gerolymos, V. Drosos, R. Kourkoulis, T. Georgarakos, and G. Gazetas, "Nonlinear response of deep immersed tunnel to strong seismic shaking," *Journal of Geotechnical and Geoenvironmental Engineering*, vol. 133, no. 9, pp. 1067–1090, 2007.
[30] I. Anastasopoulos, N. Gerolymos, V. Drosos, T. Georgarakos, R. Kourkoulis, and G. Gazetas, "Behavior of deep immersed tunnel under combined normal fault rupture deformation and subsequent seismic shaking," *Bulletin of Earthquake Engineering*, vol. 6, no. 2, pp. 213–239, 2008.
[31] A. Amorosi and D. Boldini, "Numerical modeling of the transverse dynamic behavior of circular tunnels in clayey soils," *Soil Dynamics and Earthquake Engineering*, vol. 29, no. 6, pp. 1059–1072, 2009.
[32] S. Kontoe, L. Zdravkovic, D. M. Potts, and C. O. Mentiki, "On the relative merits of simple and advanced constitutive models in dynamic analysis of tunnels," *Geotechnique*, vol. 61, no. 10, pp. 815–829, 2011.
[33] S. Kontoe, V. Avgerinos, and D. M. Potts, "Numerical validation of analytical solutions and their use for equivalent-linear seismic analysis of circular tunnels," *Soil Dynamics and Earthquake Engineering*, vol. 66, pp. 206–219, 2014.
[34] E. Bilotta, G. Lanzano, S. P. G. Madabhushi, and F. Silvestri, "A numerical Round Robin on tunnels under seismic actions," *Acta Geotechnica*, vol. 9, no. 4, pp. 563–579, 2014.
[35] G. Lanzano, E. Bilotta, G. Russo, and F. Silvestri, "Experimental and numerical study on circular tunnels under seismic loading," *European Journal of Environmental and Civil Engineering*, vol. 19, no. 5, pp. 539–563, 2015.
[36] J. Lysmer and R. L. Kuhlemeyer, "Finite dynamic model for infinite media," *Journal of Engineering Mechanics*, vol. 95, no. 4, pp. 859–877, 1969.
[37] F. Wang, X. Jiang, and J. Niu, "The large-scale shaking table model test of the shallow-bias tunnel with a small clear distance," *Geotechnical and Geological Engineering*, vol. 35, no. 3, pp. 1093–1110, 2017.
[38] F. F. Wang, X. L. Jiang, and H. Yang, "Experiment and numerical simulation study on acceleration response laws of shallow-buried small spacing tunnel with asymmetrical pressure," *Journal of Shock and Vibration*, vol. 36, no. 17, pp. 238–247, 2017.